A MECHANISTIC MODEL OF MULTIDECADAL CLIMATE VARIABILITY

by

Tyler Plamondon

A Thesis Submitted in
Partial Fulfillment of the
Requirements for the Degree of

Master of Science
in
Mathematics

May 2015

ABSTRACT

A MECHANISTIC MODEL OF MULTIDECADAL CLIMATE VARIABILITY

by

Tyler Plamondon

University of Wisconsin-Milwaukee, 2015

Under the Supervision of Dr. Sergey Kravtsov

This thesis addresses the problem of multidecadal climate variability by constructing and analyzing the output of a mechanistic model for the Northern Hemisphere's multidecadal climate variability. The theoretical backbone of our modeling procedure is the so-called "stadium-wave" concept, in which interactions between regional climate subsystems are thought to result in a phase-space propagation of multidecadal climate anomalies across the hemispheric and global scales. The current generation of comprehensive climate models do not appear to support the "stadium wave," which may indicate that either the models lack the requisite physics, or that the "stadium wave" itself is an artifact of statistical analyses used to identify it. This research aims to construct a process model that captures realistic multidecadal teleconnections between well known climatic indices, namely the North Atlantic Oscillation (NAO), Pacific Decadal Oscillation (PDO), Atlantic Multidecadal Oscillation (AMO), and El Niño/Southern Oscillation (ENSO) indices. The model is shown to predict some major components of the observed temporal structure within this climate-index network, in particular the maximum positive correlation between AMO and PDO at a +15 year lag, maximum anti-correlation between AMO and NAO at a lag of -10 years, and a peak positive correlation between the latter two indices at a +20 year lag, as well as the maximum anti-correlation between NAO and PDO at a lag of around +30 years. Future work will include exploring the model's parametric dependencies and physical feedback mechanisms leading to this behavior.

Dedicated to the author at a future time: if you are reading this and have successfully completed this document, give yourself a high-five.

TABLE OF CONTENTS

LIST OF FIGURES

LIST OF ABBREVIATIONS

AMO	**A**tlantic **M**ultidecadal **O**scillation
ENSO	**E**l-**N**iño **S**outhern **O**scillation
NAO	**N**orth **A**tlantic **O**scillation
PDO	**P**acific **D**ecadal **O**scillation
SLP	**S**ea **L**evel **P**ressure
STD	**St**andard **D**eviation
SST	**S**ea **S**urface **T**emperature
SSTA	**S**ea **S**urface **T**emperature **A**nomaly
THC	**T**hermo**h**aline **C**irculation

ACKNOWLEDGEMENTS

I would primarily like to thank my advisor, Dr. Sergey Kravtsov, for his guidance on this project. Another big thanks to my good friend, Abhilash, for his support and words of encouragement during particularly cloudy times.

Chapter 1

Introduction

The Earth's climate has gone through a warming period over the course of the 20^{th} century. Understanding the causes of this warming, how much is anthropogenically forced and how much is intrinsic, is important both scientifically and economically. This warming was nonuniform and exhibits pronounced multidecadal variations which may be a combined effect of nonlinear changes in external forcing ([2], [3], others) with global intrinsic variability superimposed on warming trends ([4], [5], others). Current climate models working towards this understanding are uncertain due to extreme sensitivity of the climate models produced to parameterizations [6].

A current attempt to understand this multidecadal variability is the "stadium wave" hypothesis ([7], [6]). It starts, theoretically, with accumulated observational and modeling evidence for the existence of the multidecadal intrinsic oscillation rooted in the dynamics of Atlantic Meridional Overturning Circulation (AMOC). It is argued [7] that this signal attains a hemispheric importance via a sequence of delayed feedbacks resulting in a "propagation" of a "wave" in a phase space of climate indices. The state-of-the-art climate models do not appear to support the stadium wave. In this study, we attempt to construct a mechanistic model that would rationalize the stadium wave.

Previously studied coupled models have been able to produce synthetic climates which exhibit intrinsic multidecadal variability in the Northern Atlantic. The global expressions of this variability, however, were typically too weak to be able to explain observed nonuniformity of the global warming rate ([8], [9]). It has been concluded that other factors must have contributed to the 20–30-yr-long mid-century pause in increasing global

temperature trends; the most likely candidate being forced climate cooling tropospheric aerosols [2].

Hemispheric signature is argued by coupled climate modelers to be weak. However, observations show a ubiquitous multidecadal signal in many climate subsystems defined using various climate indices such as AMO (Atlantic Multidecadal Oscillation), ENSO (El-Niño Southern Oscillation), NAO (North Atlantic Oscillation), and PDO (Pacific Decadal Oscillation). AMO and PDO exhibit pronounced multidecadal signals as well as annual oscillatory behavior. This multidecadal oscillation is also apparent in NAO as well as in NAO variance. ENSO does not exhibit strong multidecadal oscillations but displays a multidecadal variance component.

Building upon the work of *Tsonis et al.*, 2007 [10], recent studies [6] have considered a network of climate indices associated both dynamically and geographically with different climate subsystems. They identified oscillatory behavior with a common multidecadal time scale with varying phases across the different climatic indices. This signal propagates in the space of climate indices and the authors coined this phenomena as a "stadium wave." This wave is hypothesized to arise from the affect of AMO acting on the jet stream (NAO), which propagates a multidecadal signal to the North Pacific (PDO) and tropical Pacific (ENSO), then closing the loop over the atlantic (through NAO variance).

This thesis is structured as follows: Chapter 2 discusses the climate indices used as well as the analytical methods applied to data sets. The mechanistic model for coupled climate indices is described in chapter 3 beginning with the AMOC (Atlantic Meridional Overturning Circulation) as the major mechanism for equator-to-pole redistribution of heat. Results of the model as well as discussions of the differences and similarities between model and observed indices are presented in chapter 4. Lastly, final remarks and potential future work will be discussed in chapter 5.

Chapter 2

Data and Methods

2.1 Data

We considered a suite of well-known climate indices, which characterize the variability of oceanic and atmospheric regional climate subsystems. These subsystems (and their respective representative indices) are: Atlantic Ocean with its Meridional Overturning Circulation (AMO), Northern Hemisphere's mid-latitude jet-stream and its main jet-shifting mode (NAO), dominant mode of the North Pacific Ocean's decadal variability (PDO), as well as the famous coupled mode of tropical Pacific variability associated with ENSO.

2.1.1 Atlantic Multidecadal Oscillation (AMO)

The AMO index ([11], [12]) used here is from the NOAA's Earth System Research Laboratory [13] and was calculated from the Kaplan SST data set as an area average over the North Atlantic. The data set runs monthly from January, 1856 to March 2015.

2.1.2 Pacific Decadal Oscillation (PDO)

The PDO index ([14], [15]) used here was made available by Mantua, N.J. [16]. This index was derived as the leading principal component of monthly SST anomalies poleward of 20°N in the North Pacific Ocean. The pattern of variability was separated

from any increasing global temperature trends by removing monthly global average SST anomalies. This index runs monthly from 1900 to 2001.

2.1.3 El-Niño Southern Oscillation (ENSO)

The ENSO index ([17]) used here is the nino34 index from NOAA [18]. This index was a computation of average SSTAs across the area [5°N-5°S,170°W-120°W]. This index runs monthly from 1870 to 2015.

2.1.4 North Atlantic Oscillation (NAO)

The NAO index ([19], [20]) used here is from the NCAR/UCAR climate data guide [21]. This index is the DJFM (December, January, February, March) station-based data set. A station index for year t_i represents an average of the t_{i-1} year December value and January, February, and March of year t_i. This index runs annually from 1864 to 2014.

2.2 Data Analysis Methodology

For each time series considered, we first formed the anomalies by removing the least-squares linear trend and seasonal cycle (see section 4.1). For the latter, we regressed out the time series associated with the first five harmonics of the seasonal cycle; these time series have the form

$$\cos\left(\frac{n}{12}2\pi t\right), \quad \sin\left(\frac{n}{12}2\pi t\right) \tag{2.1}$$

where $n = 1, 2, \ldots 5$.

We calculated power spectra by means of the classical Welch periodogram method. This method slides a "window" through the time series, multiplies each window by a taper signal, calculates the Fourier transform, and computes the variance for each frequency. Each observed time series was appended ten times in order to compare results of observed and simulated data based on the default spectral estimation parameters within *Matlab*. The spectrum for model indices was computed for 100 hundred-year realizations and an ensemble average was computed to increase statistical significance (see section 4.2).

Essential to the "stadium wave" are the lagged correlations between the different members of the climate index network considered (see section 4.3). The cross-covariance of two time series, $x(t)$ and $y(t)$, is defined as

$$\sigma_{xy}(\tau) = \frac{1}{N-1}\sum_{i=0}^{N}(x(i-\tau)-\bar{x})(y(i)-\bar{y}), \tag{2.2}$$

where an overbar represents a mean value. The cross-covariance can then be normalized by dividing σ_{xy} by the STD, σ_x and σ_y, of each series to obtain the cross-correlation

$$r_{xy}(\tau) = \frac{\sigma_{xy}(\tau)}{\sigma_x \sigma_y}. \tag{2.3}$$

A value of $r_{xy} = +1$ represents perfect correlation and $r_{xy} = -1$ corresponds to perfect anti-correlation. Having a strong correlation or anti-correlation at a lagged time reveals delayed responses between signals.

Chapter 3

Mechanistic Model

3.1 AMO

The leading dynamics of the AMO here was hypothesized to be due to intrinsic variability of the Atlantic ocean Meridional Overturning Circulation [22]. Following Stommel (1961) [23], the North Atlantic ocean was modeled using two well-mixed boxes (Fig. 3.1) exchanging heat via the THC advection, wind mixing (modeled as a temperature diffusion) and driven by the heat fluxes from an overlying atmosphere. The salinity effects on circulation were neglected for simplicity.

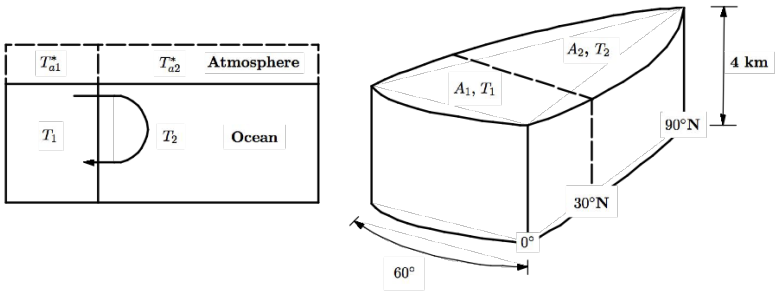

FIGURE 3.1: Qualitative representation of the Atlantic Ocean. A subscript of 1 corresponds to the south box of latitude 0°-30°N and a subscript of 2 corresponds to the north box of latitude 30°N-90°N. Upper case A refers to the surface area of the corresponding basin, and upper case T refers to temperature.

Warm water flows north in the upper layers of the Atlantic ocean followed by a southward return of cooler water in the lower layer [22]. The volume flux associated with this

overturning is parameterized, using a two-dimensional convection analogy, as

$$q \equiv k\Delta T(t - \tau_a), \tag{3.1}$$

where $\Delta T \equiv T_1 - T_2$ represents the equator-to-pole temperature gradient, k is a parameterization constant with units of $[m^3 t^{-1} K^{-1}]$, t is time in years, and τ_a is a delay. This delay is associated with a dynamical adjustment of the ocean to variable forcing.

The equations describing the evolution of each box can be written as

$$\rho c_p A h \dot{T_1} = \lambda(T^*_{a1} - T_1)A - \rho c_p |q(t)|(T_1 - T_2) - k^*_H(T_1 - T_2), \tag{3.2}$$

$$\rho c_p A h \dot{T_2} = \lambda(T^*_{a2} - T_2)A - \rho c_p |q(t)|(T_2 - T_1) - k^*_H(T_2 - T_1). \tag{3.3}$$

The air-sea heat flux is parameterized by a linearized bulk formula with the constant λ, units of $[Wm^{-2}K^{-1}]$, as $\lambda(T_a - T)$ where T_a is the radiative equilibrium temperature of the above atmosphere and T is the ocean temperature. Horizontal diffusion, characterized by the constant k^*_H, with units $[JK^{-1}t^{-1}]$, depends on the difference in temperature between the two basins. The area of each Atlantic 'box' are approximately equal, $A_1 = A_2 \equiv A$ and h represent the depth of the ocean basins. ρ is the density of water and c_p is the specific heat capacity of water.

Subtracting Eq. 3.3 from Eq. 3.2 then gives the following ODE for the temperature difference between the two basins:

$$\Delta\dot{T} = \tilde{\lambda}(\Delta T^*_a - \Delta T) - \frac{|q(t)|}{Ah}\Delta T - k_H \Delta T, \tag{3.4}$$

where $\Delta T^*_a \equiv T^*_{a1} - T^*_{a2}$, $\tilde{\lambda} \equiv \lambda/(\rho c_p h)$, and $k_H \equiv k^*_H/(\rho c_p A h)$. This model (Eq. 3.4) is driven by the specified gradient of the thermal forcing expressed via the meridional gradient of the atmospheric radiative equilibrium temperature ΔT^*_a. We postulate, that in addition to the climatological gradient, ΔT^*_a, is also influenced by the evolution of underlying SSTs via Bjerknes-style feedback, and has a substantial noise component due to atmospheric eddies.

For model tuning, it is useful to derive an expression for the Eq. 3.4 climatology under a given constant forcing ΔT^*_a. When the system is in equilibrium: $\Delta\dot{T}$=0. Then, solving

Eq. 3.4 for ΔT as $\Delta\bar{T}$ gives

$$\bar{q}(t) = k\Delta\bar{T} = -\frac{(\tilde{\lambda} + k_H) - \sqrt{(\tilde{\lambda} + k_H)^2 + \frac{4k}{Ah}\tilde{\lambda}\Delta T_a^*}}{2/(Ah)}. \tag{3.5}$$

The negative root was chosen in order to guarantee $\Delta T > 0$ in equilibrium. This means the temperature near the equator is higher than toward the arctic, as one would expect. Due to the uncertainty in λ, k_H can be taken to be zero. Solving Eq. 3.5 for k gives

$$k = \frac{\bar{q}(\frac{\bar{q}}{Ah} + \tilde{\lambda})}{\tilde{\lambda}\Delta T_a^*}. \tag{3.6}$$

Now, a noisy atmosphere is introduced (NAO, section 3.4). This can be broken up into a base forcing, Bjerknes style feedback of ocean into atmosphere [24], and white noise. The base forcing is the mean difference in radiative equilibrium temperature of the north and south atmospheres, the Bjerknes feedback is parameterized by the constant γ, and the white noise $\xi(t)$ is weighted by the amplitude A_N. Mathematically, this all is written as

$$\Delta T_a^* = \Delta\bar{T_a}^* + \gamma\Delta T + A_N\xi(t). \tag{3.7}$$

Plugging Eq. 3.7 into Eq. 3.4 then gives

$$\Delta\dot{T} = -\frac{|q(t)|}{Ah}\Delta T - \tilde{\lambda}(1-\gamma)\Delta T + \tilde{\lambda}\Delta\bar{T_a}^* + \tilde{\lambda}A_N\xi(t). \tag{3.8}$$

In order to non-dimensionalize Eq. 3.8, the following scales are defined: $[t]$ ≡1yr and $[T]$ ≡1K. Eq. 3.8 can then be multiplied through by $[t]/[T]$, absorbing $[T]$ into temperature terms, to get

$$\Delta\dot{T} = -\frac{|q(t)|}{Ah}[t]\Delta T - \tilde{\lambda}[t](1-\gamma)\Delta T + \tilde{\lambda}[t]\Delta\bar{T_a}^* + \tilde{\lambda}[t]A_N\xi(t). \tag{3.9}$$

3.1.1 AMO Parameter Choices

Begin by calculating the surface area of the Atlantic basins:

$$A_1 = \frac{\pi}{3}r_E^2\sin(30^\circ) \approx A_2 \equiv A = \frac{\pi}{3}(6.4\cdot 10^6 m)^2\sin(30^\circ) = 2.14\cdot 10^{13}m^2. \tag{3.10}$$

The depth of the oceanic layer is given in Figure 3.1 as

$$h = 4000\ m. \tag{3.11}$$

Then, initial tweaking of Eqn. 3.9 gives

$$\lambda = 30\frac{W}{m^2K} \longrightarrow \tilde{\lambda} \equiv \frac{\lambda}{\rho c_p h} = \frac{30Wm^{-2}K^{-1}}{1000kg \cdot m^{-3} \cdot 4000J \cdot kg^{-1}K^{-1} \cdot 2.14 \cdot 10^{13}m^2},$$

$$\tilde{\lambda} = 1.875 \cdot 10^{-9}\ s^{-1}.$$

The ocean feedback into the atmosphere, parameterized by γ was chosen to be

$$\gamma = 0.8.$$

The difference in radiative equilibrium atmospheric temperatures was assumed

$$\Delta\bar{T}_a^* = 15\ K.$$

The noise amplitude was chosen to be

$$A_N = 2.$$

Then, taking the mean volume flux as

$$\bar{q} = 8\ SV,$$

allows for the calculation of k via Eqn. 3.6:

$$k = 0.56\ SV \cdot K^{-1}.$$

Choosing a delay parameter of

$$\tau_a = 15\ yrs$$

then completes this model. These parameters were chosen to give comparable results with observations.

3.2 PDO

The proposed model for PDO is given as

$$\dot{T_p} = -k_a T_p - k_o T_p(t - \tau_p) + \gamma(\Delta T + A_p \xi(t)), \tag{3.12}$$

where T_p is the SST anomalies of the North Pacific, k_a is the weight of the negative feedback with dimensions of frequency, k_o is the weight of the delay effect (same dimensions as k_a), and τ_p is a delay.

The negative linear feedback of Eq. 3.12 represents atmospheric damping of SST anomalies. The choice of damping parameter k_a may reflect the air-sea exchange within particular geographical/dynamical areas such as the interactions between the Aleutian low-pressure system and the subtropical gyre circulation in the North Pacific [25].

The second term on the right-hand-side of Eq. 3.12 is a delayed suppression of SSTAs. The underlying dynamics may be attributed to adjustment via oceanic Rossby waves as a result of variable forcing.

On decadal time scales, NAO (section 3.4, AMO effect and intrinsic atmospheric noise) is zonally symmetric. It is assumed here that the Atlantic and Pacific exhibit the same atmospheric forcing. This is represented by the term in parenthesis of Eq. 3.12.

Eq. 3.12 can be made dimensionless by the same kind of argument of Eq. 3.9.

3.2.1 PDO Parameter Choices

Parameters are chosen so that simulations mimic the observed behavior in time and frequency space (spectral analysis). The delayed feedback amplitude is chosen to be

$$k_o = 0.2 \quad s^{-1},$$

the instantaneous atmospheric feedback parameter as

$$k_a = 0.8 \quad s^{-1},$$

the noise amplitude as

$$A_p = 0.8,$$

and the delay parameter as

$$\tau_p = 12 \quad yrs.$$

3.3 ENSO

ENSO has been treated as a delayed action oscillator in the past ([1], [26], etc..). This was the basis of the ENSO model here as well. The western side of the tropical Pacific has a deep thermocline which allows for SST anomalies to influence the atmosphere. The opposite is the case in the east. Shallow thermocline depth allows for the cool SSTs to be influenced by wind anomalies. This is shown schematically in Figure 3.2.

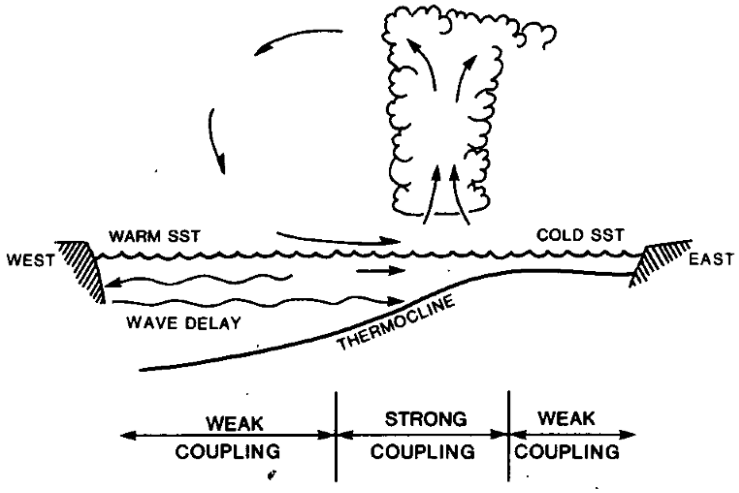

FIGURE 3.2: "In the central to eastern part of the basin, a strong positive feedback loop exists between SST anomalies, heating anomalies and surface wind anomalies. In the west, the wind-driven ocean perturbations do not affect SST; but rather perturb the deep thermocline. Uncoupled or weakly coupled waves travel to the western boundary and back to the east, where they affect the SST."[1]

The ENSO model is given as

$$\dot{T}_e = k_e T_e - b T_e^3 - D' T_e(t - \tau_e(t)) + A_e \Gamma(t), \tag{3.13}$$

where T_e represents tropical SST anomalies, k_e is the parameterization of positive feedback, b is the nonlinear suppression coefficient, D' is weight of delayed negative feedback, A_e is the white-noise amplitude, Γ represents Gaussian white-noise, and τ_e is a delay.

The first term of Eq. 3.13 is known as the Bjerknes feedback for ENSO ([26], [1]). This is the byproduct of the coupled ocean-atmosphere dynamics in the Pacific. Positive perturbations of SSTs in the east from a flat thermocline reduces the Walker circulation which leads to an even flatter thermocline and further warming of SSTs.

Without any sort of suppression, the positive Bjerknes feedback would allow for SST anomalies to grow without bound. Nonlinear effects, such as advective processes (primarily; [27],[1]) in the ocean and moist processes in the atmosphere act to limit this. An exact form is not known, so this nonlinear suppression takes a cubic form.

Equatorially trapped ocean waves propagate westward as Rossby waves. These waves reflect as eastward propagating Kelvin waves and bring the opposite thermocline depth anomaly to the east coast of the Pacific with a delay τ_e.

Warm ENSO events tend to occur when PDO is in a positive phase and cool ENSO events when PDO's phase is negative. PDO effects the structure of the thermocline in the equatorial Pacific and this changes the Rossby and Kelvin wave propagation speeds. In this respect, $\tau_e = \tau_e(t)$. Assuming a constant background delay $\bar{\tau}_e$, the time dependence of τ_e is then assumed

$$\tau_e(t) = \bar{\tau}_e + sT_p(t), \tag{3.14}$$

where s is the amplitude for the modulation of ENSO's delay parameter by PDO.

Scaling Eq. 3.13, time by the time $k_e t$ and temperature by $\sqrt{b/k_e}T_e$, allows the equation to be written in dimensionless form as

$$\dot{T}_e = T_e - T_e^3 - DT_e(t - \tau_e(t)) + A_e\Gamma(t), \tag{3.15}$$

where $D \equiv D'/k_e$. Because A_e is just a noise amplitude, it did not get redefined. T_e, t, and τ_e in Eq. 3.15 are now dimensionless.

3.3.1 ENSO Parameter Choices

Attempting to create ENSO patterns with periods of rapid and weak oscillations on similar time scales as the observed ENSO, the linear positive-feedback frequency was

chosen to be

$$k_e = 0.1 \quad yr^{-1},$$

the nonlinear damping coefficient as

$$b = 0.1 \quad K^{-2} yr^{-1},$$

the amplitude of delayed feedback from equatorially trapped waves as

$$D' = 1 \quad yr^{-1},$$

the mean delay of the trapped waves as

$$\bar{t}_e = 10 \quad months,$$

and the amplitude that modulates the delay of ENSO as

$$s = 2.$$

These parameters differ significantly from those chosen in previous literature ([26], [1]). This model is not meant to be an exact realization of the ENSO effect, so the parameter choices are not definite. The above values of k_e and b are are an order of magnitude less than previously used values [26]. Also, setting $D' = 1$ implies no loss of information upon reflection of Rossby waves from the eastern Pacific basin. This is not physical. However, this model is not derived from first principles and the above parameters seem to give a more realistic ENSO-type behavior such as periods of increasing and decreasing variance.

3.4 NAO

The proposed NAO model is

$$P_a = -\gamma \Delta T + (1 - \epsilon) A_N \xi(t) + \epsilon T_e, \tag{3.16}$$

where P_a represents the difference in SLP anomalies between the sub-tropical and sub-polar regions of the Atlantic and ϵ is a weight. Equation (3.16) is dimensionless by construction.

The SLP across the Atlantic will have a significant contribution from the SSTs governed by AMO. This can be characterized by the Bjerknes feedback and is the first term in the right-hand-side of (3.16). This means positive ΔT anomalies tend to decrease this pressure difference, and vice versa.

A recent study [28] suggests that ENSO influences the Atlantic atmosphere. This can be added to the model in an ad-hoc way by combining ENSO with the noise in the Atlantic atmosphere from AMO using the wight ϵ.

The only new parameter in NAO to be chosen is ϵ. This is taken to be

$$\epsilon = 0.85$$

in order to produce similar temporal patterns between the model and observations (see section 4.1).

3.5 The mechanistic model of coupled oscillators

The model constructed in this section is thus the one for a sequence of coupled delayed action oscillators, each of which in isolation represents dynamics of various climate subsystems: AMO, NAO, PDO and ENSO. The AMO behavior affects the NAO via air–sea coupling, and the NAO transfers this AMO signal to the Pacific, thus introducing multidecadal time scales into PDO. PDO, in turn, affects the ENSO behavior, which feeds back on the NAO. To close this system, we should let the ENSO-driven NAO component (see the last term in 3.16) to affect the AMO as forcing in (3.9). We haven't done it yet, so the results discussed below are for the sequence of one-way coupled oscillators, with ENSO's effects on AMO suppressed.

Chapter 4

Results and Discussion

The model was integrated using the standard forward Euler method. The integration step sizes were as follows:

- AMO : 1 year,
- PDO : 6 months,
- ENSO : 1 month,
- NAO : 1 year.

All observed indices are linearly detrended with the first five harmonics of the natural cycle removed in order to isolate the anomalies. Dimensionless indices were formed by dividing each index by its STD. This normalization was also performed on the model indices.

It turns out that the simulated NAO and PDO indices exhibit systematic phase-shift biases relative to other indices when compared to the observed shifts. This is clearly a drawback of our model that will need to be corrected in the future. However, we will demonstrate in this section that the manual shifting of the simulated NAO index by 10 yr forward and the PDO index — by 12 yr backward results in the best match of the simulated data's lagged cross-correlation functions with those of the observed data In summary, the reconstructions of NAO and PDO were manually shifted to compare behavior of lagged correlations between different indices (see section 4.3). A total of 102 hundred-year realizations were constructed from Eqns. 3.9, 3.12, 3.15, and 3.16.

For the manual shifting, the single time series' (10,200 years) have the beginning (end) selected years appended to the end (beginning), depending on the direction of the shift (see section 4.1). Then, the first and last hundred-year segments are discarded before breaking each long time series into one hundred 100-year sets. This gives no unphysical discontinuities in the samples.

4.1 Simulated and Observed Climate Variability

Figure 4.1 displays a sample realization of AMO as well as the observed AMO index. It is seen that the model displays similar multidecadal behavior but is not as noisy on an annual time scale (see spectral analysis of section 4.2).

As described above, the realization of PDO was manually shifted backwards by one full delay τ_p and is plotted in Figure 4.2 along with the observed 6-month mean values of the PDO index (note that the apparent match of the phase between the observed and simulated data is completely accidental). All subsequent analysis of the constructed PDO time series is done with the shifted data. To the naked eye, these two time series share very similar traits but further analysis is required to better understand this.

A sample realization of the ENSO (unshifted) model is shown in Figure 4.3. Note that the model, just like observations, shows prolonged decadal periods of strong and frequent ENSO events.

Finally, a sample of the NAO reconstruction is plotted with the annually observed NAO index. The NAO reconstruction was shifted 10 years forward (see above) to match correlations found between AMO and NAO in observations (Section 4.3).

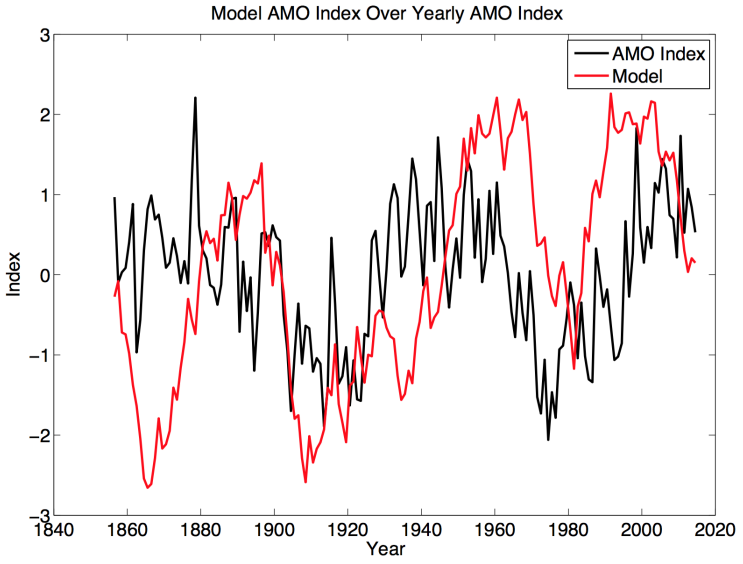

FIGURE 4.1: Sample model realization of AMO plotted with observed annual-mean values of AMO.

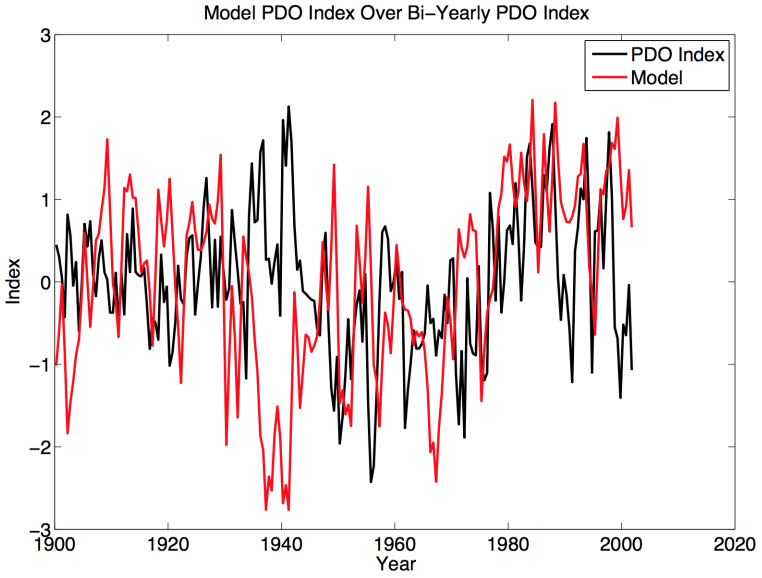

FIGURE 4.2: Sample model realization of PDO plotted with observed annual-mean values of PDO.

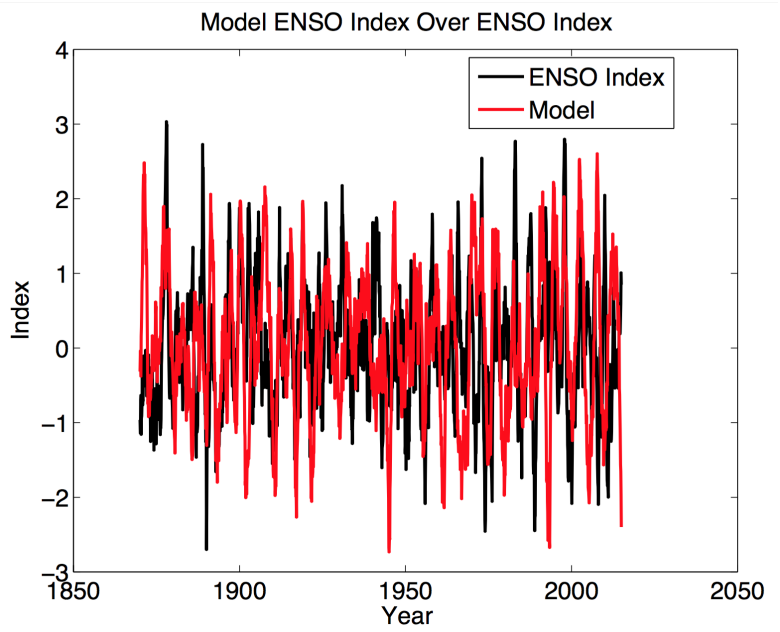

FIGURE 4.3: Sample model realization of ENSO plotted with observed monthly values of ENSO.

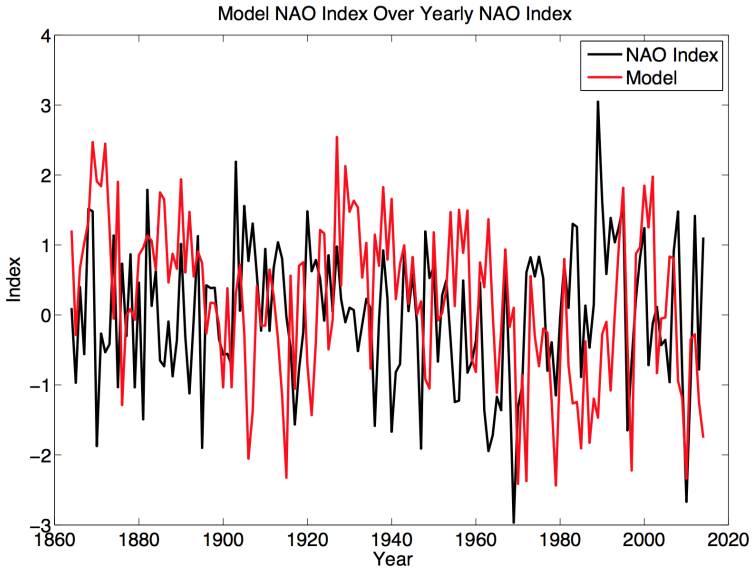

FIGURE 4.4: Sample model realization of NAO plotted with observed annual values of AMO.

4.2 Spectral Analysis

The computed spectral densities of both, observed AMO and model AMO, are plotted in Figure 4.5. The observed AMO spectrum exhibits focused energy in the 50-85 year period range with a small source at about 25 years. The model primarily describes dominant periods on the bounds of this range along with a trail of periods into the 25 year range, but not including a significant signal at a period of 25 years.

The PDO model comes close to resolving the three leading periods of the PDO index at ∼60, ∼25, and ∼9 years. This is shown in Figure 4.6. The observed PDO has a strong source of energy around a period of ∼5.5 years that the model is missing.

The observed ENSO spectrum, shown in Figure 4.7, is fairly noisy in the period range of 2-12 years with a small source of energy in the 1.4–1.8 year period range. The model has a much smoother distribution of frequencies in the low frequency range with a peak period of about 5 years. The energy diminishes quickly among frequencies higher than this peak. The model is missing oscillations with a period less than 2.5 years.

The observed NAO has peak periods of ∼35 and ∼85 years, as seen in Figure 4.8, whereas the model also has peak frequencies near these values, the dominant period of 50 years is a clear consequence of the AMO forcing (see Figure 4.5) .

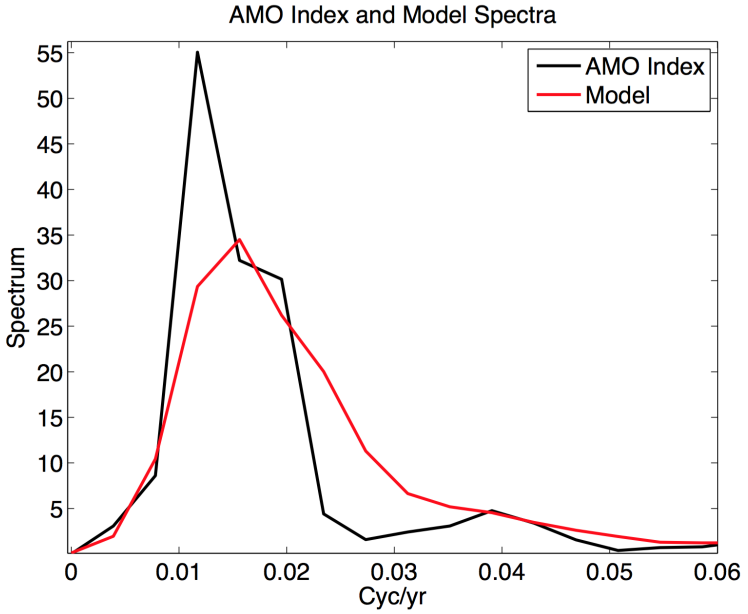

FIGURE 4.5: Spectral densities for observed AMO and model AMO. Model AMO spectral density computed as ensemble average of 100 hundred-year realizations.

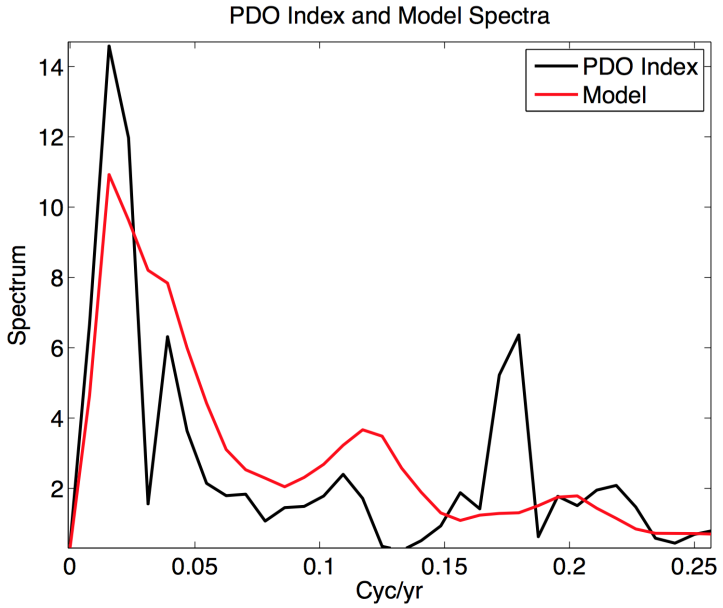

FIGURE 4.6: Spectral densities for observed PDO and model PDO. Model PDO spectral density computed as ensemble average of 100 hundred-year realizations.

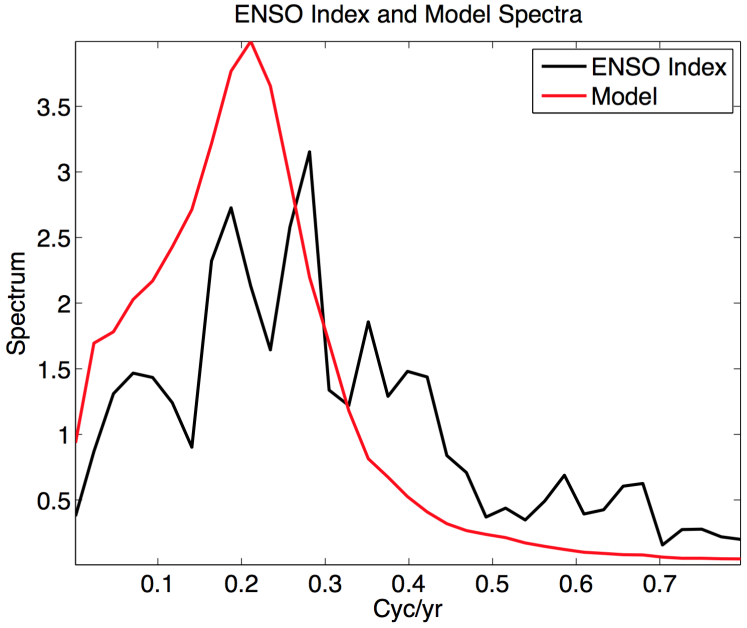

FIGURE 4.7: Spectral densities for observed ENSO and model ENSO. Model ENSO spectral density computed as ensemble average of 100 hundred-year realizations.

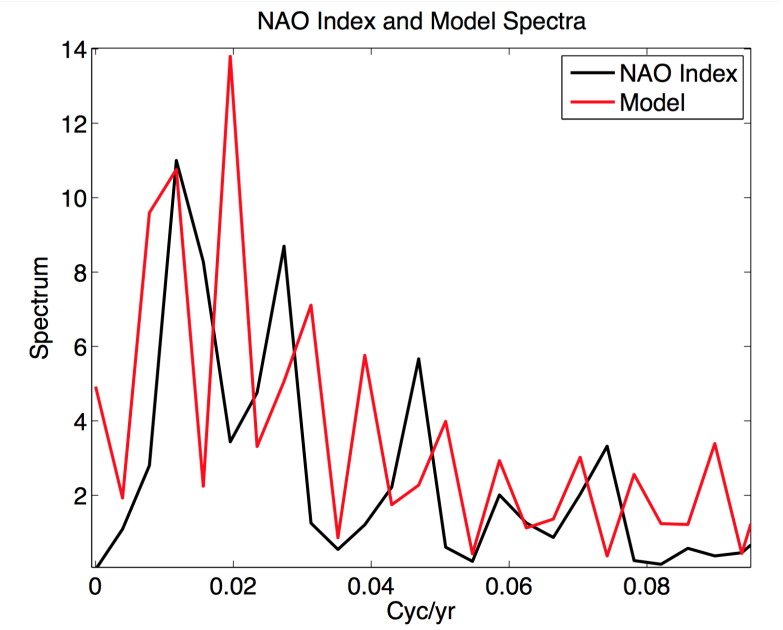

FIGURE 4.8: Spectral densities for observed NAO and model NAO. Model NAO spectral density computed as ensemble average of 100 hundred-year realizations.

4.3 Correlations

4.3.1 Smooth Indices

In order to study the correlation of multidecadal trends in the data, both observed indices and constructed indices were run through a 40-year lowpass Butterworth filter. This is shown in Figures 4.9 and 4.10. As a reminder, the NAO and PDO constructions of Figure 4.10 have been shifted (see section 4.1). These multidecadal waves are the basis of current studies into the "stadium wave" hypothesis. This is a currently debated topic. While some are looking into possible mechanisms, such as [6] and this thesis, others believe this multidecadal telloconnection to be a product of applied statistics [29].

4.3.2 Cross-Correlation of Indices

The first correlation shown in Figure 4.11 is the correlation of AMO with PDO (model PDO shifted). The observed indices demonstrate a slightly negative correlation ($\sim$-0.1) at zero lag. With increasing lag comes an increase in correlation up to a maximum positive correlation of $\sim$0.7 at a lag of about 15 years. Decreasing the lag from zero results in an increase in negative correlation until the lag reaches -15 years at which the correlation is about -0.9. The model creates this same sort of increasing positive correlation when moving from a lag of zero to a lag of about 13-15 years, where the model reaches a maximum positive correlation of 0.65-0.97. There is much more noise in the model when the lag is becoming negative. The strong anti-correlation between these indices is not captured. Because both of these model indices have been shifted, this teleconnection is not inherent in this model. Instead, Figure 4.11 highlights the similarities and differences between observed and constructed indices in the space of lag times. Further study is needed to rectify this issue.

The correlation of AMO with NAO (model NAO shifted) is shown in Figure 4.12. At a lag of -12 years, the observed AMO and NAO are maximally anti-correlated at $\sim$-0.77. The model also has a maximum anti-correlation in the -10 to -12 year lag range. The spread of this anti-correlation is between -0.6 and -0.97. This lag range is surrounded by decreasing anti-correlation in both directions. However, more than 10 lag years in

either direction from this minimum starts becoming noisy in the model and thus does not explain the strong positive correlation between AMO and NAO at lags of -45 years and 21 years. Again, these similarities and differences are relative to the manual shifts in the AMO and NAO models.

At zero lag, observed NAO is most positively correlated with PDO with a correlation of ∼0.88 (see Figure 4.13). This correlation is underestimated by the model (both indices shifted) with a wide uncertainty ranging into negatively correlated values. The maximum anti-correlation occurs at a lag of about 30 years. The model estimates this at a lag of ∼26 years and the spread remains negative. The secondary maximum of anti-correlation of the observed indices occurs at a lag of about -37 years. Similar to the situation about a lag of zero, the model is very noisy in this region and does not capture this occurrence. With both of these model indices shifted, these similarities are not directly inherent in the model.

The reader has been reminded several times of the manual shift in the realizations of NAO and PDO. Because of these shifts, it was mentioned that the shown teleconnections in Figures 4.11, 4.12, and 4.13 are not strictly inherent in the model. However, it was the single shift of PDO by 12 years and NAO by 10 years which resulted in the best correspondence between observed and model correlations for all simulated realizations. This suggests the model may be capable of producing the correct lag correlations between indices with either: further adjustment of parameters, introduction of additional relevant lags, or introducing missing dynamics such as adding atmospheric forcing to AMO and PDO by means of ENSO's effect on NAO.

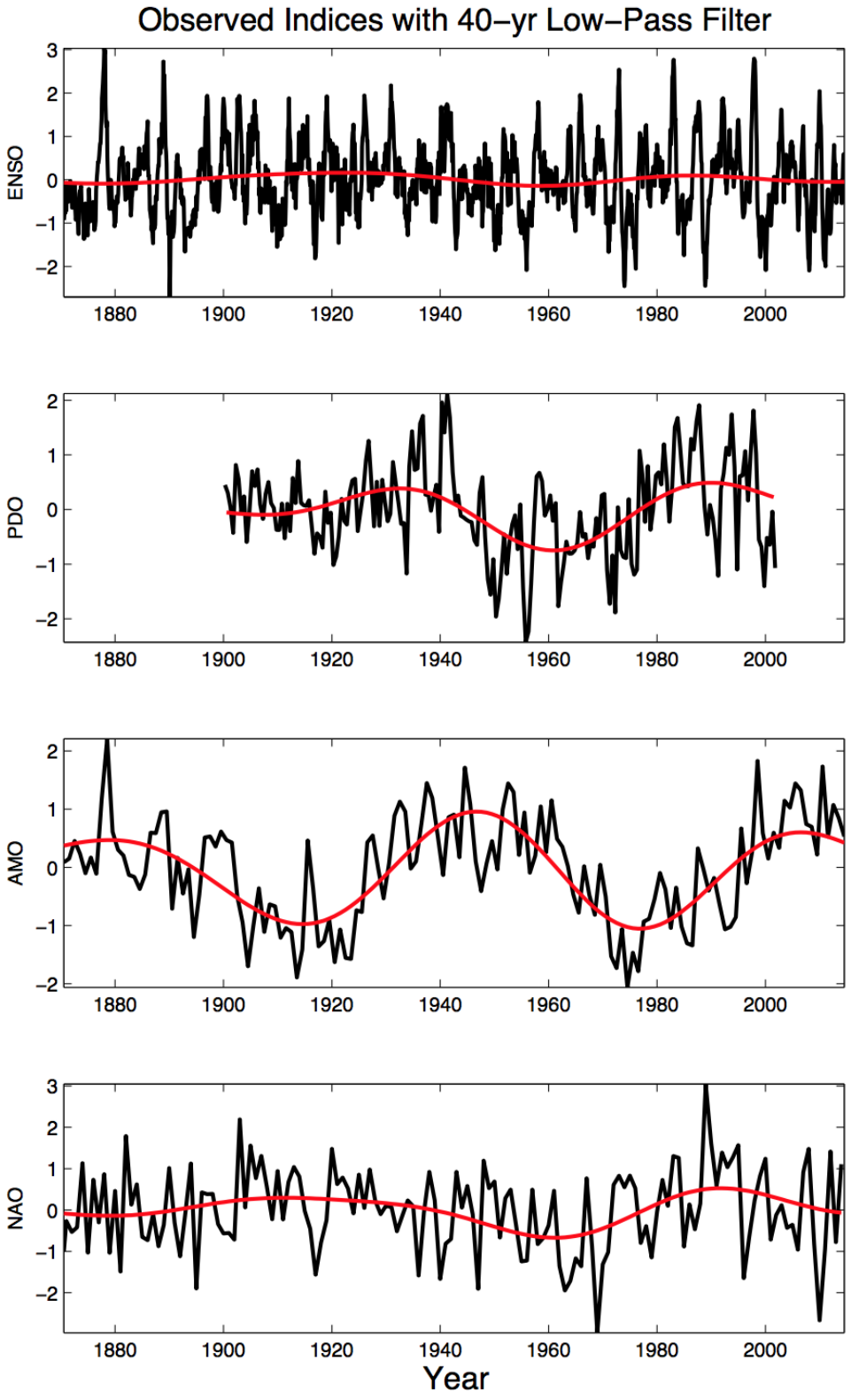

FIGURE 4.9: Observed indices (black) with smoothed indices (red) plotted on top. The smoothed indices were computed by means of a 40-year lowpass filter.

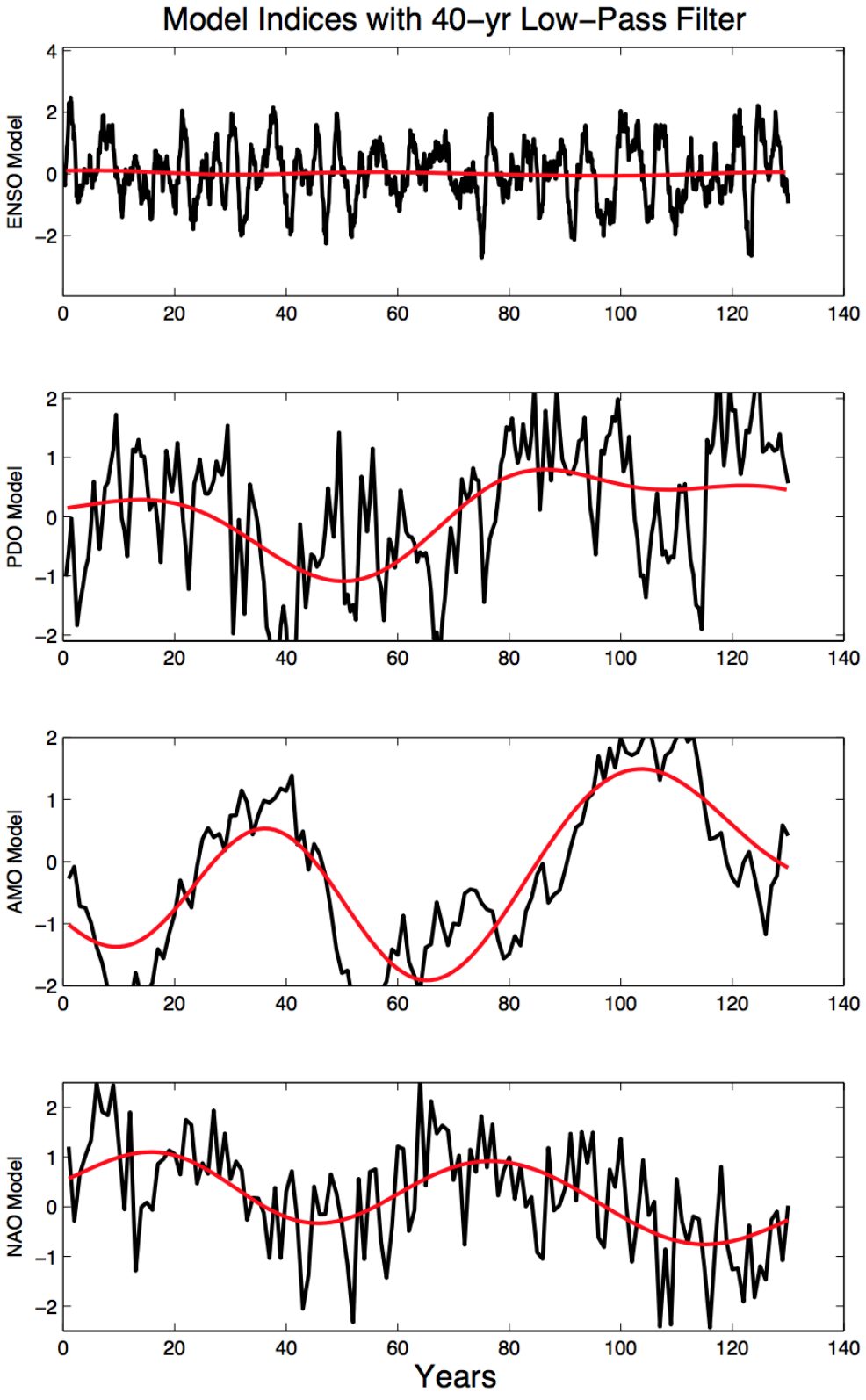

FIGURE 4.10: Model indices (black) with smoothed indices (red) plotted on top. The smoothed reconstructions were computed by means of a 40-year lowpass filter.

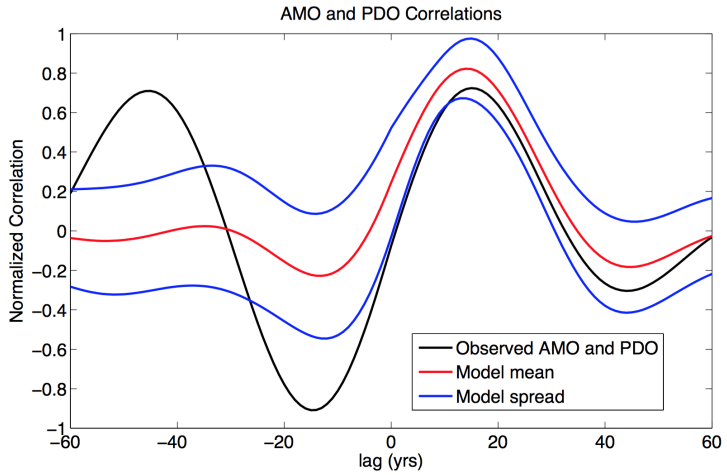

FIGURE 4.11: Correlation between smoothed AMO and PDO indices. Observed (black) and model (red). PDO model index has been shifted as described in the text. The model spread (blue) is the ±STD of the correlation calculated over one hundred 100-year correlations.

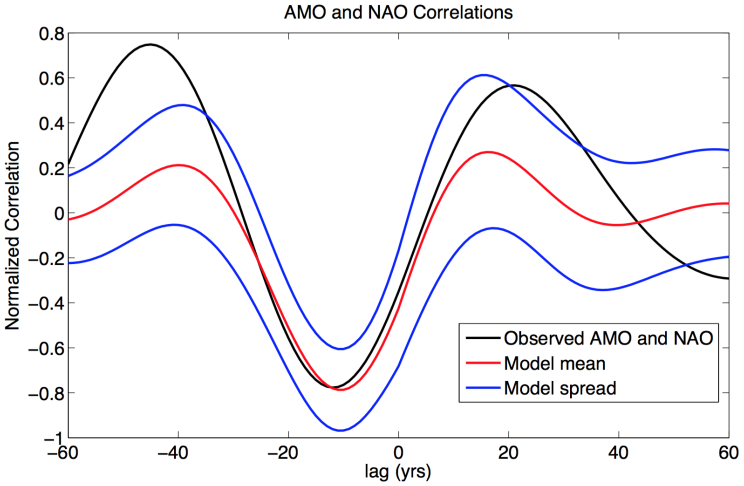

FIGURE 4.12: Correlation between smoothed AMO and NAO indices. Observed (black) and model (red). NAO model index has been shifted as described in the text. The model spread (blue) is the ±STD of the correlation calculated over one hundred 100-year correlations.

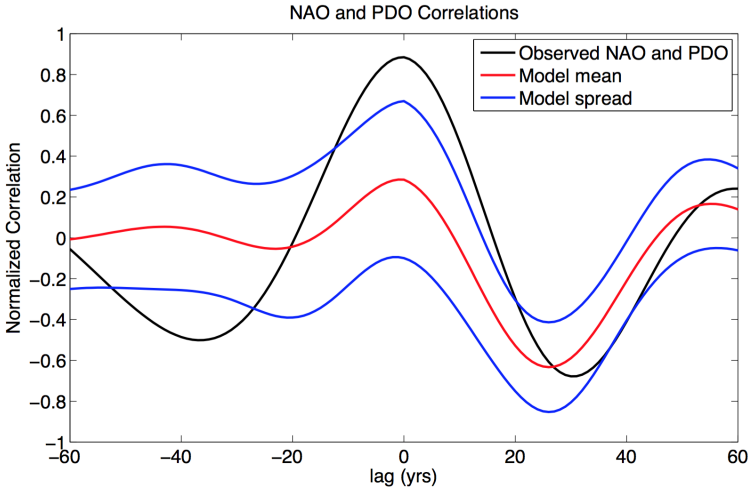

FIGURE 4.13: Correlation between smoothed NAO and PDO indices. Observed (black) and model (red). Both model indices have been shifted as described in the text. The model spread (blue) is the ±STD of the correlation calculated over one hundred 100-year correlations.

Chapter 5

Conclusions and Future Work

We examined collective multidecadal variability in the observed and simulated indices representing different sub-systems of the grand climate system. In particular, the dynamics of the Atlantic Ocean's Meridional Overturning Circulation (AMOC) manifests in multidecadal oscillations of the Atlantic Multidecadal Oscillation (AMO) SST index (North Atlantic area-averaged SSTs [11]). The North Atlantic SST redistribution is hypothesized to affect the the mid-latitude jet stream, whose latitudinal shifts recorded in the variability of the North Atlantic Oscillation (NAO) index [21] communicate the multidecadal AMOC signal to the Pacific Ocean. This signal is used to drive the noisy atmosphere of the Pacific Decadal Oscillation's (PDO) SSTAs poleward of 20°N ([14], [16]). The PDO effects the thermocline structure across the equatorial Pacific which changes the wave propagation speed of equatorially trapped Rossby and Kelvin waves, one of the primary driving mechanisms of the SSTAs across the equatorial Pacific known as the El-Ñino Southern Oscillation (ENSO) [18]. This dynamical sequence, referred to as the stadium wave [6] was modeled mechanistically in a suite of coupled delayed oscillator models representing each subsystem.

Observed climate indices were linearly detrended with the first five harmonics of the natural seasonal cycle removed in order to isolate anomalies from global warming and periodic seasonal trends. Both observed and model indices were normalized by their respective STDs to compare dimensionless time series. Power spectra by means of the Welch periodogram were computed for observed and constructed series. To increase statistical significance of model index spectra, one hundred 100-year time series were

used to compute an ensemble average. Observed and model date sets were smoothed using a 40-year lowpass Butterworth filter. This smoothing highlights the multidecadal components of the indices, particularly AMO, NAO, and PDO. The normalized cross-correlation of indices was then computed from the smoothed versions of observed and model indices.

Our model produces realizations which have similar temporal behaviors as those of observed indices. AMO is dominated by a multidecadal component in the model but is lacking in variance on a yearly time-scale. Model PDO demonstrates positive and negative phases on the multidecadal scale from the influence of AMO as well as realistic decadal variations. ENSO realizations display multidecadal variations in amplitude variance which correspond to periods of El-Niño and La-Niña ([27], [28]). The realization of NAO demonstrates realistic oscillatory amplitudes on yearly time scales as driven by ENSO as well as a multidecadal component.

From the realizations (with the previously described shifts), we demonstrate the model's potential in describing some strong correlations between observed indices. AMO and PDO have a strong positive correlation at a lag of about 15 years which is resolved by the the shifted PDO index with statistical significance. The correlation between these indices surrounding a lag of 15 years is also similar but becomes noisy in the model. The peak anti-correlation between AMO and NAO is found at a lag of -15 years which is resolved from the shifted NAO index with statistical significance. The model becomes particularly noisy when moving to positive lags. NAO and PDO display strong positive correlation at a lag of zero years, which the model also demonstrates but not with statistical significance. The strong anti-correlation at a lag of about 30 years is more statistically resolved by the model but closer to a lag of about 25 years.

Before computing the normalized cross-correlation between smoothed AMO/PDO, AMO/-NAO, and NAO/PDO, the realizations of NAO and PDO were shifted in order to compare the dependence of the correlations on lag time of the model results with observations. A single shift of 12 years backwards for PDO and 10 years forward for NAO. While shifting the data in this fashion doesn't demonstrate intrinsic multidecadal teleconnections from within the model, the fact that this single shift gives the most realistic comparison with observations does demonstrate that there may be a key component of the model missing or a parameter adjustment is required.

In the future, we plan on introducing the ENSO-driven NAO component to affect the AMO forcing. We hope this will increase statistical significance in correlation between model climate indices as well as account for strong connections seen in observations which were not present within simulations. As well as improving the present results, we hope to demonstrate the multidecadal components of ENSO and NAO variance which may be helpful in predicting future El-NiÑo and La-Niña events.

Bibliography

[1] Max J. Suarez and Paul S. Schopf. A delayed action oscillator for enso. *J. of Atmospheric Sciences*, 45, November 1988. URL http://journals.ametsoc.org/doi/pdf/10.1175/1520-0469%281988%29045%3C3283%3AADAOFE%3E2.0.CO%3B2.

[2] Tatsuya Nagashima, Hideo Shiogama, Tokuta Yokohata, and Toshihiko Takermura. Atlantic multidecadal oscillation and northern hemisphere's climate variability. *Geophysical Research Letters*, L04702, February 2006. URL https://www.image.ucar.edu/~nychka/IDAG/Papers/Nagashima_carbonaceous_aerosols.pdf.

[3] Ben B. B. Booth, Nick J. Dunstone, Paul R. Halloran, Timothy Andrews, and Nicolas Bellouin. Aerosols implicated as a prime driver of twentieth-century north atlantic climate variability. *Nature*, 484:228–232, April 2012. URL http://www.nature.com/nature/journal/v484/n7393/full/nature10946.html.

[4] C. K. Folland, D. E. Parker, and F. E. Kates. Worldwide marine temperature fluctuations 1856–1981. *Nature*, 310:670–673, August 1984. URL http://www.nature.com/nature/journal/v310/n5979/abs/310670a0.html.

[5] M. Ghil and R. Vautard. Interdecadal oscillations and the warming trend in global temperature time series. *Nature*, 350:324–327, March 1991. URL http://www.nature.com/nature/journal/v350/n6316/abs/350324a0.html.

[6] Sergey Kravtsov, Marcia G. Wyatt, Judith A. Curry, and Anastasios A. Tsonis. Two contrasting views of the multidecadal climate variability in the twentieth century. *Geophysical Research Letters*, 41:6881–6888, October 2014.

[7] Marcia Glaze Wyatt, Sergey Kravtsov, and Anastasios A. Tsonis. Atlantic multidecadal oscillation and northern hemisphere's climate variability. *Climate Dynamics*, pages 929–949, March 2011. URL http://link.springer.com/article/10.1007%2Fs00382-011-1071-8.

[8] Jeff R. Knight, Robert J. Allan, Chris K. Follan, Michael Vellinga, and Michael E. Mann. A signature of persistent natural thermohaline circulation cycles in observed climate. *Geophysical Review Letters*, 32(L20708), 2005. doi: 10.1029/2005GL024233.

[9] Thomas L. Delworth, Rong Zhang, and Michael E. Mann. *Decadal to centennial variability of the atlantic from observations and models, in past and future changes of the oceans meridional overturning circulation: mechanisms and impacts*, volume 173. AGU, Washington, D.C., 2007.

[10] A. A. Tsonis, K. Swanson, and S. Kravtsov. A new dynamical mechanism for major climate shifts. *Geophysical Review Letters*, 34(L13705), 2007. doi: 10.1029/2007GL030288.

[11] A. Kaplan, M. Cane, Y. Kushnir, A. Clement, M. Blumenthal, and B. Rajagopalan. Analyses of global sea surface temperature 1856-1991. *Journal of Geophysical Research*, 103:18,567–18,589, 1998.

[12] R. W. Reynolds and T. M. Smith. Improved global sea surface temperature analyses. *Journal of Climate*, 7, 1994.

[13] NOAA: Earth System Research Laboratory. Amo (atlantic multidecadal oscillation) index. http://www.esrl.noaa.gov/psd/data/timeseries/AMO/, 2015.

[14] Y. Zhang, J. M. Wallace, and D. S. Battisti. Enso-like interdecadal variability: 1900-93. *Journal of Climate*, 10:1004–1020, 1997.

[15] N. J. Mantua, S. R. Hare, Y. Zhang, J. M. Wallace, and R. C. Francis. A pacific interdecadal climate oscillation with impacts on salmon production. *Bulletin of the American Meteorology Society*, 78:1069–1079, June 1997. URL http://www.atmos.washington.edu/~mantua/abst.PDO.html.

[16] Nathan Mantua. Pdo index. ftp://ftp.atmos.washington.edu/mantua/pnw_impacts/INDICES/PDO.latest, 2002.

[17] N. A. Rayner, D. E. Parker, E. B. Horton, C. K. Folland, V. Alexander, D. P. Rowell, E. C. Kent, and A. Kaplan. Global analyses of sea surface temperature, sea ice, and night marine air temperature since the late nineteenth century. *Journal of Geophysical Research*, 108(D14), 2003. doi: 10.1029/2002JD002670.

[18] NOAA PSD. Nino34. http://www.esrl.noaa.gov/psd/gcos_wgsp/Timeseries/Data/nino34.long.data, 2015.

[19] J. W. Hurrell. Decadal trends in the north atlantic oscillation: Regional temperatures and precipitation. *Science*, 269:676–679, 1995.

[20] J. W. Hurrell and C. Deser. North atlantic climate variability: the role of the north atlantic oscillation. *Journal of Marine Systems*, 78(1):28–41, 2009.

[21] NCAR and UCAR. Hurrell north atlantic oscillation (nao) index (station-based). https://climatedataguide.ucar.edu/climate-data/hurrell-north-atlantic-oscillation-nao-index-station-based, 2015.

[22] U.S. Geological Survey and Peter Saundry. Atlantic meridional overturning circulation. http://www.eoearth.org/view/article/150290/, 2010.

[23] Henry Stommel. Thermohaline convection with two stable regimes of flow. *Tellus*, 13:224–230, 1961.

[24] J. Bjerknes. Atlantic air-sea interaction. *Adv. Geophys.*, 10:1–82, 1964.

[25] M. Latif and T. P. Barnett. Causes of decadal climate variability over the north pacific and north america. *Science*, 266(5185):634–637, January 1994. URL http://www.atmos.washington.edu/~rennert/etc/courses/pcc587/ref/latif-barnett.pdf.

[26] Ian. Boutle, Richar H. S. Taylor, and Rudolf A. Römer. El niño and the delayed action oscillator. *Am. J. Phys*, 75, 2007. URL http://scitation.aip.org/content/aapt/journal/ajp/75/1/10.1119/1.2358155.

[27] M. A. Cane and S. E. Zebiak. A theory for el niño and the southern oscillation. *Science*, 228(4703):1085–1087, May 1985.

[28] Wenjun Zhang, Lei Wang, Baoqiang Xiang, Li Qi, and Jinhai He. Impacts of two types of la niña on the nao during boreal winter. *Climate Dynamics*, 44:1351–1356, March 2015.

[29] Byron A. Steinman, Michael E. Mann, and Sonya K. Miller. Atlantic and pacific multidecadal oscillations and northern hemisphere temperatures. *Science*, 347 (6225):988–991, February 2015.